Current Biology, Vol. 15, 1701–1711, October 11, 2005, ©2005 Elsevier Ltd All rights reserved. DOI 10.1016/j.cub.2005.08.035

The Heparan Sulfate Proteoglycan Syndecan Is an In Vivo Ligand for the *Drosophila* LAR Receptor Tyrosine Phosphatase

A. Nicole Fox and Kai Zinn*
Broad Center
Division of Biology
California Institute of Technology
Pasadena, California 91125

Summary

Background: Receptor tyrosine phosphatases (RPTPs) are essential for axon guidance and synaptogenesis in *Drosophila*. Each guidance decision made by embryonic motor axons during outgrowth to their muscle targets requires a specific subset of the five neural RPTPs. The logic underlying these requirements, however, is still unclear, partially because the ligands recognized by RPTPs at growth cone choice points have not been identified. RPTPs in general are still "orphan receptors" because, while they have been found to interact in vitro with many different proteins, their in vivo ligands are unknown.

Results: Here we use a new type of deficiency screen to identify the transmembrane heparan sulfate proteoglycan Syndecan (Sdc) as a ligand for the neuronal RPTP LAR. LAR interacts with the glycosaminoglycan chains of Syndecan in vitro with nanomolar affinity. Genetic interaction studies using *Sdc* and *Lar* LOF mutations demonstrate that Sdc contributes to LAR's function in motor axon guidance. We also show that overexpression of Sdc on muscles generates the same phenotype as overexpression of LAR in neurons and that genetic removal of LAR suppresses the phenotype produced by ectopic muscle Sdc. Finally, we show that there is at least one additional, nonproteoglycan, ligand for LAR encoded in the genome.

Conclusions: Taken together, our results demonstrate that Sdc on muscles can interact with neuronal LAR in vivo and that binding to Sdc increases LAR's signaling efficacy. Thus, Sdc is a ligand that can act in *trans* to positively regulate signal transduction through LAR within neuronal growth cones.

Introduction

Signaling through tyrosine phosphorylation is essential for axon guidance. Two large families of enzymes, protein tyrosine kinases (PTKs) and protein tyrosine phosphatases (PTPs), directly control phosphorylation of axonal proteins on tyrosine residues. Many of the PTPs are receptor-like molecules (RPTPs) that have extracellular domains related in sequence to cell-adhesion molecules (CAMs), connected via a single transmembrane domain to either one or two cytoplasmic PTP domains.

The structural similarity of RPTPs to receptor tyrosine kinases (RTKs) has led to the hypothesis that extracellular ligands modulate RPTP activity, as they do with RTKs. To date, however, RPTPs are still "orphan receptors" because, while they have been found to interact with many different proteins, their physiologically relevant ligands are unknown (reviewed by [1]). The only RPTP-ligand interaction that has been shown to have an effect on signaling is that of RPTP-β/ζ with the secreted growth factor pleiotrophin/HB-GAM; pleiotrophin binding increases phosphorylation of β-catenin in cell culture [2]. RPTP-β/ζ binds to a number of other proteins in vitro as well, including known CAMs (reviewed by [3]).

Several RPTPs can mediate homophilic adhesion, suggesting that they function as their own ligands (reviewed by [1]). The mammalian LAR RPTP can bind to a laminin-nidogen complex [4]. Finally, and most relevant to the present study, in vitro binding studies have shown that heparin and heparan sulfate proteoglycans (HSPGs) directly interact with avian RPTPσ, a close relative of LAR. This same RPTP also binds to a non-HSPG protein in muscle [5]. However, it is unknown whether HSPGs or the muscle protein contribute to RPTPσ function in vivo [6].

Drosophila has provided a unique system for investigation of the in vivo roles of RPTPs during neural development (reviewed by [7]). The fly genome encodes six RPTPs, five of which are selectively expressed in neurons. Genetic studies of these five neural RPTPs have shown that they are required for axon guidance and synaptogenesis during both embryonic and larval stages.

Embryonic motor axons navigate to their muscle targets along five major nerve pathways (ISN, ISNb, ISNd, SNa, and SNc; see http://www.its.caltech.edu/~zinnlab/motoraxons/fma%20home%20page.html for diagrams and images of the motor axon/muscle system). Analysis of motor axon guidance phenotypes in *Rptp* single mutants and mutant combinations has revealed that each growth cone guidance decision made by motor axons requires a specific subset of the five neural RPTPs [8–13]. Most *Rptp* single mutant phenotypes are partially penetrant, because several RPTPs can participate in each guidance decision. To generate a highly penetrant alteration in motor axon guidance, it is usually necessary to remove a specific combination of two or more RPTPs.

The combinatorial roles of RPTPs in regulating specific guidance decisions could be explained by a model in which ligands for particular RPTPs are located near each growth cone choice point and that these control the specificity of RPTP function. In this model, a particular RPTP might participate in an axon guidance decision only if its ligand is contacted by the relevant growth cones at the time at which they are making the decision.

The RPTP LAR is involved in guidance of ISNb motor axons at the entrance to their target ventrolateral muscle (VLM) field. In *Lar* mutants, these axons leave the common ISN pathway at the "exit junction" but then fail to enter the VLM field to innervate their muscle targets.

*Correspondence: zinnk@caltech.edu

Instead, they continue to grow dorsally in a bundle adjacent to the common ISN pathway.

In this paper, we employ a deficiency screen to identify a cell-surface HSPG, Syndecan (known as Sdc in *Drosophila*) [14], as an in vivo ligand for LAR. Syndecans are cell-surface HSPGs that have transmembrane regions. However, they can also be cleaved to produce free extracellular domains that are shed into the medium. Another class of cell-surface HSPGs, the glypicans, is attached to the membrane via glycosyl-phosphatidylinositol (GPI) linkages (reviewed by [15]).

Syndecans consist of an extracellular core protein domain of ~250 amino acids (aa) to which long glycosaminoglycan (HS-GAG) side chains are attached, followed by a transmembrane domain and a short cytoplasmic domain. The GAG chains are composed of repeating disaccharide units that are sulfated at specific positions. They are attached, polymerized, and modified by a complex biosynthetic pathway involving the activities of many different enzymes.

HSPGs are involved in many different cellular processes, among which are adhesion, motility, proliferation, differentiation, and morphogen transport. In *Drosophila*, the glypicans Dally and Dally-like (Dlp) are required for Hedgehog and Wingless singnaling (reviewed by [15, 16]). Cell-surface HSPGs can function as receptors for soluble ligands, as ligands for receptors on adjacent cell surfaces, and as coreceptors for other transmembrane signaling proteins on the same cells. HSPGs shed into the medium can act as soluble ligands for receptors on surrounding cells.

HSPGs also have roles in axon guidance. They work together with FGF signaling to control axon guidance in the *Xenopus* visual system and are required for attraction of growth cones to Semaphorin 5A (reviewed by [17, 18]). HSPGs also regulate axon guidance via the Slit/Robo pathway in *Drosophila* and zebrafish [19–21].

Our findings in this paper provide a new mechanism for HSPG-mediated axon guidance. We identified Sdc in a screen for ligands of the *Drosophila* LAR RPTP and characterized its interactions with LAR by using biochemistry and genetics. Our results indicate that Sdc expressed on muscles can positively regulate LAR signaling in motor neurons.

Results

A Deficiency Screen for Genes Encoding LAR Ligands

To search for ligands of the *Drosophila* RPTPs, we first devised an in vivo staining procedure based on the affinity probe techniques developed by Flanagan and colleagues (reviewed by [22]). For LAR, the entire extracellular domain of the protein (consisting of three immunoglobulin-like [Ig] domains and nine fibronectin type III [FN] repeats) was fused to human placental alkaline phosphatase (PLAP), and the resulting fusion, LAR-AP, was expressed as a secreted protein using the baculovirus system.

To detect and localize putative LAR ligands, live-dissected stage 16 embryonic filets were incubated with LAR-AP in the absence of nonionic detergent, followed by fixation and probe detection using secondary and fluorescent tertiary antibodies (see Supplemental Experimental Procedures available with this article online). Incubation of wild-type filets with LAR-AP reveals a complex staining pattern, including CNS axons (Figure 1B), intense stripes of staining at muscle attachment sites in the periphery (Figure 1C), and a segmentally repeated pattern of midline and exit glia in the CNS (Figure 1A). The muscle attachment site and glial staining patterns have distinctive dot-like morphologies. We also generated and tested similar AP fusion proteins for the DPTP10D, DPTP99A, and DPTP69D RPTPs, and we found that each produces a distinctive staining pattern on live embryo filets (A. Schmid, A.N.F., and K.Z., unpublished results). Unconjugated PLAP and a variety of other AP fusion proteins exhibited no specific binding to embryos (Figure S1, Table S1).

To identify the genomic region(s) encoding the putative LAR ligands responsible for this staining pattern, we dissected and stained live embryos homozygous for each of the deletion mutations in the Bloomington Stock Center deficiency kit, which at that time contained about 225 lines. We identified a second chromosome deletion, *Df(2R)AA21*, which eliminated the bright peripheral LAR-AP staining at muscle attachment sites and also removed most of the dot-like glial staining. CNS axons were still stained in deletion embryos, however.

By performing complementation crosses with overlapping deletions and staining embryos from these crosses with LAR-AP, we were able to narrow down the region required for staining to a small interval (57E1–9) just proximal to the *Egfr* gene. The interval contains only four identified genes: *Sdc*, *Sara*, *Fkbp13*, and *MESK2* (Figure 1J).

Syndecan Is a Ligand for LAR

Sdc, a transmembrane HSPG, was the logical candidate for the LAR ligand encoded in this region, because it is the only predicted cell-surface protein. Furthermore, an avian LAR ortholog had already been shown to bind to HSPGs [6]. To test this hypothesis, we examined *Sdc* mutant embryos for LAR-AP staining. We used three different *Sdc* mutations. $Sdc^{Df(2R)48}$ is a ~20 kb deletion that removes N-terminal *Sdc* coding region and also deletes all or part of the *Sara* and *Fkbp13* genes [20]. Sdc^{10608} and $Sdc^{KG06163}$ are independent P element insertion mutations in an *Sdc* intron (Figure 1J). All three of these mutations eliminated the dot-like LAR-AP staining of muscle attachment sites and glia (Figures 1D and 1E, Table S1). Mutations in *Sara* or *Fkbp13* had no effect on LAR-AP staining (Table S1).

Sdc mRNA and protein are expressed in a variety of tissues in the embryo [14, 20, 21]. Strikingly, Sdc protein is expressed at high levels in a dot-like pattern at muscle attachment sites, and this pattern appears identical to that component of the peripheral LAR-AP staining pattern that is eliminated by *Sdc* mutations (compare Figures 1C and 1G). Sdc is also expressed at high levels on CNS axons (Figure 1F), which stain with LAR-AP. However, staining of CNS axons by LAR-AP is retained in zygotic *Sdc* mutants (Figure 1D), although staining for Sdc is greatly reduced (Figures 1H and 1I), indicating that other putative LAR ligand(s) are also localized to axons (see below).

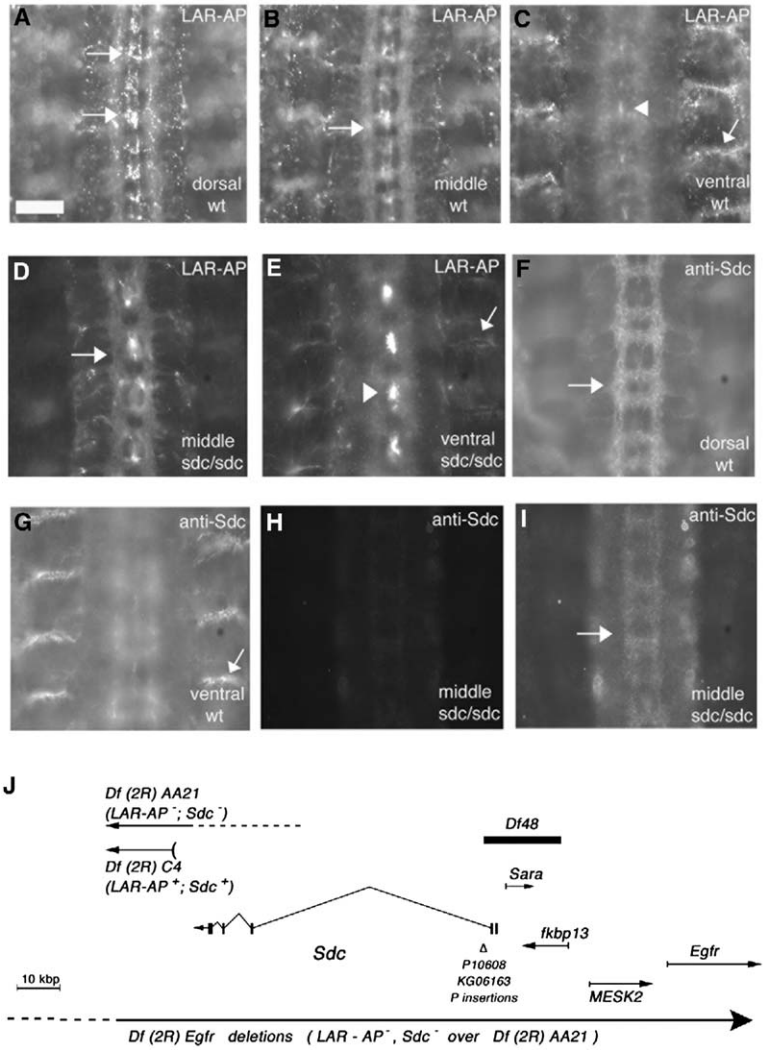

Figure 1. LAR-AP Staining of *Drosophila* Embryos Identifies Sdc as a LAR Binding Protein

Each image shows four abdominal segments of the CNS and the ventral muscle region in a live-dissected stage 16 embryo filet; anterior is up. Staining is visualized with immunofluorescence (40× objective). The muscle attachment sites shown are at the ends of the longitudinal ventral (15, 16, 17) and ventrolateral (7, 6, 13, 12) muscles. Scale bar equals 10 μm.

(A–C) Three focal planes of LAR-AP staining of a wild-type embryo filet.

(A) LAR-AP, dorsal (top) focal plane. Arrows indicate midline glia.

(B) LAR-AP, middle focal plane. Arrow indicates staining of CNS longitudinal tracts.

(C) LAR-AP, ventral (deep) focal plane. Arrowhead indicates staining of ventral CNS midline cells; arrow indicates muscle attachment site staining. Note the characteristic dot-like morphology of the muscle attachment site staining.

(D and E) LAR-AP staining of an $Sdc^{KG06163}$ embryo filet.

(D) Middle focal plane, showing that staining of the CNS axon ladder is still prominent (arrow). The axon ladder is somewhat distorted; this is the *Sdc* phenotype.

(E) Ventral focal plane, showing that peripheral staining at muscle attachment sites is greatly reduced (arrow). Arrowhead: ventral CNS midline cells.

(F and G) Anti-Sdc staining of a wild-type embryo filet.

(F) Dorsal focal plane, showing that Sdc is expressed on CNS axons (arrow).

(G) Ventral focal plane, showing bright dot-like anti-Sdc staining of muscle attachment sites (arrow). Note that this pattern is essentially identical to the LAR-AP attachment site staining in (C).

(H) Anti-Sdc staining of an Sdc^{Df48} (zygotic null) embryo filet, using the same exposure time as (F) and (G). Sdc protein levels are much reduced.

(I) A much longer exposure of anti-Sdc staining of the same embryo filet, demonstrating that maternally contributed Sdc protein still localizes to CNS axons (arrow).

(J) A map of the *Sdc-Egfr* region. *Df(2R)AA21* lacks peripheral LAR-AP staining and anti-Sdc staining. *Df(2R)C4* retains LAR-AP and anti-Sdc staining. The mapped breakpoint of *AA21* is to the left of the *C4* breakpoint, but our results show that it must actually lie to its right, within *Sdc*. *Df(2R)Egfr5* deletes *Egfr* and extends to the left. The Sdc^{10608} and $Sdc^{KG06163}$ insertions are both located near the 5′ end of the large *Sdc* intron. Sdc^{Df48} was generated by imprecise excision of Sdc^{10608}.

LAR-AP staining of muscle attachment sites can be blocked by adding excess heparin, a highly sulfated form of HS. This implies that LAR-AP interacts with Sdc through its HS-GAG side chains, rather than with the Sdc protein core. In keeping with this, LAR-AP binding to the periphery is eliminated in embryos mutant for *sulfateless (sfl)*, *sugarless (sgl)*, and *tout-velu (ttv)* (Figure S1, Table S1). These genes encode enzymes that are necessary for GAG chain synthesis and sulfation, and HSPG levels are reduced in zygotic mutant larvae lacking each of these enzymes [23].

The *Drosophila* genome encodes two other cell-surface HSPGs, the glypicans Dally and Dally-like (Dlp) [24, 25]. There is also a Perlecan, an extracellular matrix HSPG, encoded by the *trol* gene [26, 27]. To examine whether any of these proteins contribute to the LAR-AP staining pattern observed on wild-type embryos, we stained *dally* single mutants, *dally dlp* double mutants, and *trol* mutants. No changes from the normal staining pattern were observed (Figure S1, Table S1).

To further demonstrate that LAR-AP interacts with Sdc, we ectopically expressed Sdc in muscles and showed that this ectopic muscle Sdc can be recognized by LAR-AP. LAR-AP was also able to bind to the glypican Dally when it was expressed at high levels on muscles (Figure S2).

Evidence for a Second LAR Ligand

In *Sdc* mutants, while the bright dot-like LAR-AP staining at muscle attachment sites is absent, staining of CNS axons is still prominent (Figure 1D). There are also faint double lines extending into the periphery in each

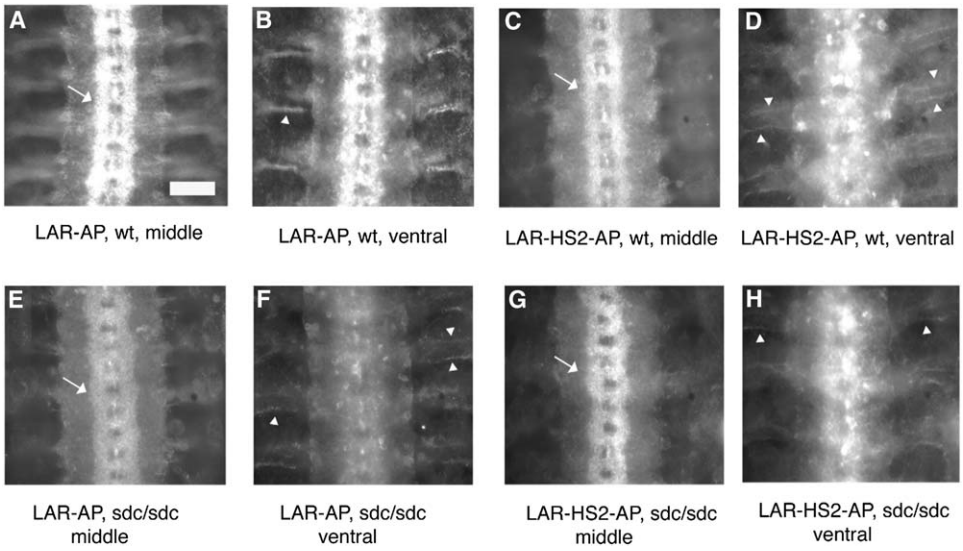

Figure 2. A Heparan Sulfate Binding-Defective LAR-AP Protein, LAR-HS2-AP, Stains CNS Axons and Peripheral Lines in *Sdc* Mutant Embryos

Images of stage 16 embryo filets like those in Figure 1. Scale bar equals 10 μm.

(A) LAR-AP staining of wild-type embryo, middle focal plane, showing CNS axons (arrow).

(B) LAR-AP, same wild-type embryo as (A), ventral focal plane, showing muscle attachment site staining (arrowhead).

(C) LAR-HS2-AP, wild-type, middle focal plane, showing CNS axons (arrow).

(D) LAR-HS2-AP, same wild-type embryo as (C), ventral focal plane. Note the absence of bright dot-like staining in the periphery. This has been replaced by faint double lines extending into the periphery in each segment (arrowheads).

(E) LAR-AP, *Sdc* maternal/zygotic mutant embryo, middle focal plane, showing CNS axons (arrow).

(F) LAR-AP, same *Sdc* mutant embryo as (E), ventral focal plane, showing faint double lines in the periphery (arrowheads). Note that this pattern is almost identical to that in (D), indicating that the remaining LAR-AP staining in the absence of Sdc is the same as that seen with an HS binding-defective mutant in wild-type.

(G) LAR-HS2-AP, *Sdc* maternal/zygotic mutant embryo, middle focal plane, showing CNS axons (arrow).

(H) LAR-HS2-AP, same *Sdc* mutant embryo as (G), ventral focal plane, showing faint double lines in the periphery (arrowheads). Note that this pattern is also like that in (D), indicating that the HS binding-defective mutant binds in the same manner to wild-type embryos and to embryos lacking Sdc.

hemisegment, which probably correspond to specific muscle edges or attachment sites (Figure 2F, arrowheads). The residual staining in *Sdc* mutants is resistant to heparin, suggesting that it is mediated by a non-HSPG protein. This protein is not LAR itself, because staining of CNS axons is unchanged in *Lar* null mutant embryos (Table S1).

To characterize interactions with the putative second, non-HSPG, LAR ligand(s), and to further prove that LAR-AP interacts with Sdc through its GAG chains, we expressed mutant versions of LAR-AP with point mutations in putative HS binding motifs in the first Ig domain. Such mutants would be expected to be unable to interact with Sdc but might bind normally to non-HSPG ligands.

We made two mutants that we predicted would eliminate HS binding based on sequence analysis and on the RPTPσ mutants made by [6]. The canonical HS binding motif is BBXBB (B = K or R) [28]. In LAR-HS1-AP, we mutated the motif ^{61}RKNGKK^{66} to ^{61}AANGAA^{66}. In LAR-HS2-AP, the basic cluster ^{101}RAGR^{104} was mutated to ^{101}AAGA^{104}. AP fusion proteins were produced for both mutants, and results reported below show that these do not bind well to heparin or HSPGs.

Figures 2C and 2D show two focal planes of staining of wild-type embryo filets with LAR-HS2-AP. This protein stains CNS axons and double lines in the periphery; the pattern in the periphery is quite distinct from that seen with LAR-AP (compare to Figure 2B). To prove that this staining pattern is independent of Sdc, we made maternal/zygotic *Sdc* mutant embryos that lack any detectable Sdc protein. This can be done by crossing *Sdc^{Df48}, ubi-Sara/Sdc^{10608}* females (in which *Sara* function is rescued by a transgene, allowing survival) to *Sdc^{Df48}, ubi-Sara/CyO-GFP* males. When these embryos are stained with LAR-AP (Figures 2E and 2F) or LAR-HS2-AP (Figures 2G and 2H), an identical pattern of staining is observed with the two fusion proteins. Similar results were obtained with LAR-HS1-AP (Table S1). In summary, these findings indicate that at least one other cell-surface-associated protein can interact with the extracellular domain of LAR and that this interaction is not mediated through HS GAGs. This second LAR ligand (or ligands) is expressed on CNS axons and in a distinct pattern in the periphery.

LAR Interacts with Sdc and Heparin In Vitro

We characterized interactions of LAR and the other RPTPs with HS in vitro using a solid-phase binding assay with heparin-agarose beads. In this assay, beads were mixed with each AP fusion protein at the same fusion protein concentration (approximately 2 nM), so that the extent of binding reflects the relative affinity of each fusion protein for the beads. These results showed

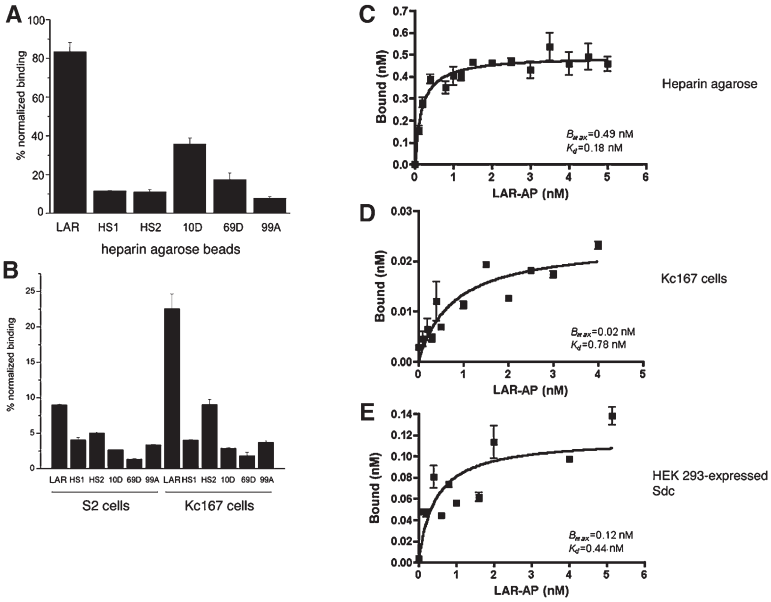

Figure 3. In Vitro Binding of LAR-AP to Heparin-Agarose Beads, *Drosophila* Cells, and Recombinant Sdc

(A) Bar graph of binding of RPTP-AP fusion proteins to heparin-agarose beads. Bound protein/total protein (calculated from assays of AP activity) is expressed as a percentage. Fusion proteins are at an approximate concentration of 2 nM. LAR-AP binds well to heparin-agarose beads, while much less binding is observed with the HS1 and HS2 mutants and the other RPTP-APs.

(B) Bar graph of binding of RPTP-AP fusion proteins to *Drosophila* S2 and Kc167 cells. Conditions as in (A). ~3-fold more LAR-AP binding is observed with Kc167 cells than with S2 cells, while the other AP proteins bind similarly to S2 and Kc167 cells.

(C–E). Saturation binding curves. Heparin-agarose beads (C), Kc167 cells (D), and supernatant from Sdc-FLAG-expressing human 293T cells (E) were incubated with the indicated concentrations of LAR-AP. The mean and standard error of three measurements of bound LAR-AP are plotted. Best fit binding curves (solid lines) were calculated by linear regression analysis to derive the indicated K_ds and extrapolated maximum binding values.

that LAR-AP exhibits at least 8-fold more binding than the HS1 and HS2 mutants discussed above. If we assume that HS1 and HS2 binding reflects the level of nonspecific interaction with the beads (the HS1 mutation eliminates the only canonical HS binding motif in LAR), this leads to the conclusion that DPTP69D and DPTP99A do not bind specifically to heparin-agarose. However, some binding of DPTP10D-AP over background is observed in this assay (Figure 3A).

We then performed similar experiments with two *Drosophila* cell lines: Kc167, which makes Sdc at high levels, and S2, which makes very little Sdc [14]. The binding profile with Kc167 cells was similar to that seen with heparin-agarose, except that the HS2 mutant exhibited more binding than HS1 and DPTP10D-AP did not bind (Figure 3B). For S2 cells, LAR-AP bound at 3-fold lower levels than to Kc167 cells, while the other proteins bound at levels similar to those seen with Kc167 cells. These data suggest that Kc cells bind to LAR-AP through Sdc. Kc167 cells do express mRNAs for the glypicans Dally and Dlp, so glypican binding could contribute to LAR-AP's interactions with Kc167 cells. However, we found that treatment of Kc167 cells with phosphatidylinositol-specific phospholipase C, which releases glypicans from the cell surface by cleaving GPI linkages, did not reduce binding of LAR-AP (data not shown).

We then performed saturation binding experiments with heparin-agarose beads, Kc167 cells, and FLAG-tagged secreted Sdc made in human 293T cells. The binding plots are shown in Figures 3C–3E. We calculated affinities from these plots using nonlinear regression fitting of the data to a single-site binding model. This method has been shown to yield more accurate calculated affinities than Scatchard analysis when the two methods are compared side by side using the same primary data [29]. The calculated K_d value for LAR-AP binding to heparin-agarose is 0.18 nM (Figure 3C). For Kc167 cells, it is 0.78 nM (Figure 3D). Finally, analysis of binding of LAR-AP to secreted, FLAG-tagged *Drosophila* Sdc from 293T cell supernatants yielded a K_d of 0.44 nM (Figure 3E). The calculated K_d values obtained from our experiments are very similar to those determined by Aricescu et al. in their analysis of HSPG binding to the avian LAR ortholog RPTPσ. The K_d values derived from their experiments were 0.32 nM (heparin), 0.18 nM (agrin), and 0.21 nM (collagen XVIII) [6].

We were also able to coimmunoprecipitate LAR-AP and Sdc by mixing LAR-AP protein with supernatant from *Sdc*-FLAG-transfected HEK 293T cells, precipitating the secreted Sdc with anti-FLAG, and detecting LAR-AP by immunoblotting with anti-PLAP (Figure S3). In summary, these results indicate that LAR binds selectively to HS and to Sdc in vitro.

Sdc Contributes to LAR's Motor Axon Guidance Function

Lar mutants display a characteristic motor axon guidance phenotype called ISNb bypass [8, 10]. ISNb axons normally innervate the VLM field, including muscles 6, 7, 12, and 13. These axons initially fasciculate with the common ISN pathway, exiting the CNS via the ISN root. They then leave the ISN at the exit junction and grow into the muscle field (Figures 4A, 4B, and 4D). In *Lar* mutant embryos, ISNb axons successfully split away from the ISN pathway at the exit junction, but then some or all of these axons fail to grow into the muscle field at their normal entry point. Instead, they travel along parallel to the ISN, underneath the muscles, until they reach the dorsal edge of the VLM field (Figures 4C, 4E, and 4F). Zygotic null *Lar* mutant embryos display a complete or partial ISNb bypass phenotype with a

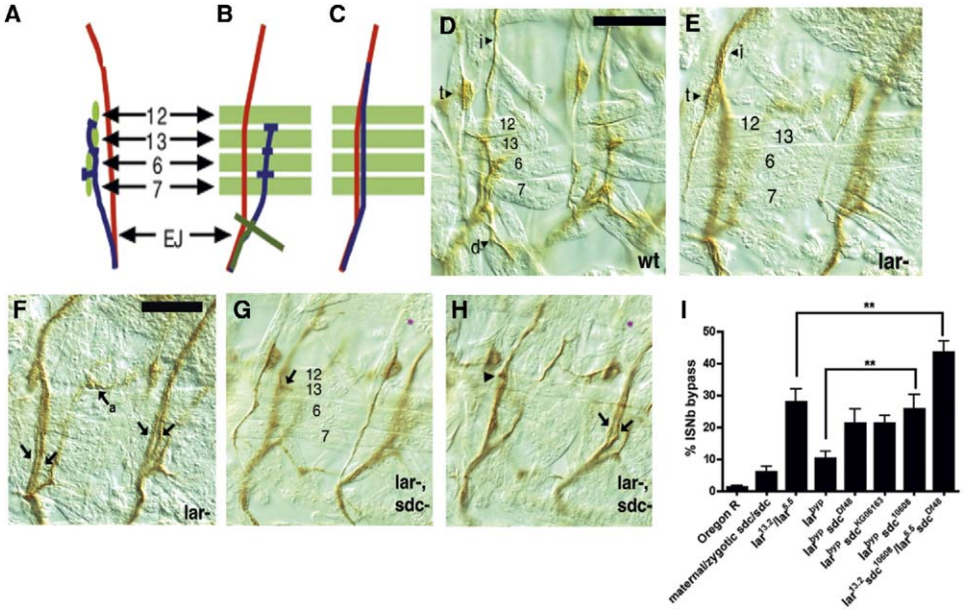

Figure 4. Sdc Participates in LAR-Mediated ISNb Axon Guidance

(A–C) Schematic diagrams of ISNb axons and their muscle targets at late stage 16. The ISNb is blue, ISN is red, ISNd is dark green, and the VLMs (numbered) are light green. Dorsal is at top.

(A) Normal ISNb pathway, side view (internal to left). The ISNb leaves the ISN at the exit junction (EJ) and turns inward to target the VLMs. It is thus in a more superficial focal plane than the ISN when viewed from the internal side (as in a filet preparation).

(B) Top view, like that seen in a filet preparation. The ISNb has begun to form synapses on the VLMs (horizontal bars). The ISNd extends along the axis of the ventral muscles.

(C) The bypass phenotype characteristic of *Lar* mutants, top view. The ISNb leaves the ISN but then fails to enter the muscle field and grows along parallel to the ISN and in the same (external) plane. The ISNd does not extend.

(D–H) Each panel shows two abdominal hemisegments of a late stage 16 embryo filet stained with mAb 1D4 using HRP immunohistochemistry and visualized with DIC optics (63× objective). Dorsal is at top and anterior to left. Muscles 6, 7, 12, and 13 are labeled in some panels. i, ISN; d, ISNd; t, transverse nerve; a, SNa. Scale bars equal 5 μm. Scale bar in (D) is also used for (E); scale bar in (F) is also used for (G) and (H).

(D) Hemisegments A5 and A6 of a wild-type embryo. The focal plane is at the level of the VLMs. Note that the ISNb is in the same focal plane as the muscles, while the ISN is out of focus under the VLMs.

(E and F) Bypass phenotype, in hemisegments A5 and A6 of a $Lar^{13.2}/Lar^{5.5}$ embryo.

(E) The focal plane is at the level of the VLMs. Note that no axons are in focus, because the ISNb is now under the VLMs.

(F) The focal plane is at the level of the ISN, external to (under) the muscles. The ISNb and ISN are seen as two parallel bundles in both hemisegments (arrows); the ISNb appears to rejoin the ISN near the dorsal edge of the VLMs.

(G and H) Bypass phenotype, in hemisegments A5 and A6 of a $Lar^{13.2}$ $Sdc^{10608}/Lar^{5.5}$ Sdc^{Df48} embryo.

(G) The focal plane is at the level of the VLMs. Note that the ISNb is out of focus, because it is under the VLMs. However, a "foldback" branch of the ISNb (arrow) has grown back ventrally from the ISNb after it passed under the VLMs and is forming a synapse on muscle 13.

(H) The focal plane is at the level of the ISN, under the muscles. The ISNb and ISN are seen as two parallel bundles in the right hemisegment (arrows); the ISNb appears to rejoin the ISN near the dorsal edge of the VLMs. The arrowhead indicates the point at which the foldback axon(s) leave the ISNb to grow back over the VLMs.

(I) A bar graph showing the % of A2–A7 hemisegments that exhibit partial or complete ISNb bypass in various genotypes. The numbers of hemisegments scored are as follows: *Oregon R* = 395; Sdc^{Df48}, *ubi-Sara*/Sdc^{Df48} maternal/zygotic mutant (see text) = 240; $Lar^{13.2}/Lar^{5.5}$ = 332; Lar^{bypass} = 211; Lar^{bypass} Sdc^{Df48} = 171; Lar^{bypass}, $Sdc^{KG06163}$ = 263; Lar^{bypass}, Sdc^{10608} = 163; $Lar^{13.2}$ $Sdc^{10608}/Lar^{5.5}$ Sdc^{Df48} = 273; $^{**}p < 0.01$.

penetrance of 25%–30% (i.e., 25%–30% of A2-A7 abdominal hemisegments in late stage 16 embryos have ISNb axons that bypass the VLMs). This penetrance can also be influenced by maternal genotype, suggesting that some *Lar* function is provided maternally. When mothers bearing *Df(2L)E55*, which removes N-terminal *Lar* coding sequence and may act as a dominant negative, are crossed to males bearing a null *Lar* point mutation, the penetrance of the bypass phenotype increases to ~70% [8, 10].

To determine whether Sdc's interactions with LAR are important for ISNb axon guidance, we studied genetic interactions between *Lar* and *Sdc*. We first examined embryos homozygous for each of the three *Sdc* alleles described above (zygotic *Sdc* mutants), as well as maternal/zygotic *Sdc* mutants, and we found that they display ISNb bypass at frequencies only slightly greater than in wild-type (Figure 4I, Figure S4A). We then combined the three *Sdc* mutations with three different *Lar* mutations and evaluated whether the penetrance of the ISNb bypass phenotype in these double mutants was increased above the levels observed in the corresponding *Lar* single mutants.

We initially made double mutants with each of the three *Sdc* mutations together with the hypomorphic allele Lar^{bypass}, for which the bypass phenotype occurs

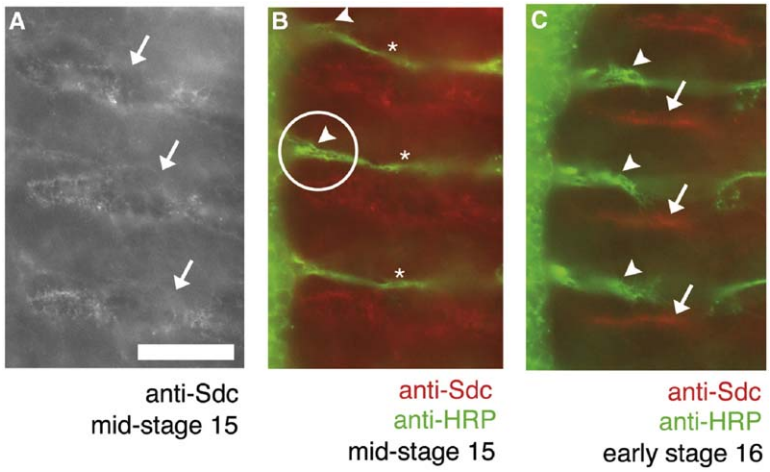

Figure 5. Sdc Is Expressed on Cells Adjacent to the Motor Nerves at the Appropriate Time to Influence ISNb Guidance

Live-dissected embryo filets were stained with anti-Sdc (red) and anti-HRP (green) to visualize the motor nerves (40× objective). Hemisegments A3–A5 are shown. Anterior is up and ventral to left. Scale bar equals 5 μm.

(A) Anti-Sdc staining alone, in a mid-stage 15 embryo. Arrows indicate patches of staining between the motor nerves.

(B) Merge of anti-Sdc and anti-HRP staining (same anti-Sdc image). The circle shows the region of the exit junction/muscle field entry site; arrowheads indicate growth cones in this vicinity. Note that the Sdc patches are immediately posterior to the motor nerves. The bright green structure to the left of images (B) and (C) is the edge of the CNS. Asterisk indicates ISN.

(C) Sdc and anti-HRP, in an early stage 16 embryo. The broad patches of Sdc staining have become narrower and are farther from the motor nerves (arrows); these will converge to the muscle attachment site staining seen in Figure 1. The ISNb has formed a distinct pathway within the VLM field by this time (arrowheads).

at a penetrance of about 10%. This mutation introduces a frame shift that causes deletion of the second PTP domain [30]. These double mutants had bypass phenotypes indistinguishable from those in *Lar* mutants and did not display any new motor axon guidance phenotypes. For each of the *Sdc* alleles, the bypass penetrance in the double mutants is increased by more than 2-fold above that seen for Lar^{bypass}. The largest effect is observed for Sdc^{10608}, where penetrance increases from 10% in Lar^{bypass} to 26% in Lar^{bypass} Sdc^{10608} (Figure 4I; $p < 0.01$).

We also combined Sdc^{Df48} and Sdc^{10608} with $Lar^{13.2}$ and $Lar^{5.5}$, which are early stop codon (presumed null) mutations, and evaluated bypass phenotypes in the resultant double transheterozygote. These double mutants displayed an increased penetrance of the bypass phenotype (43%; Figures 4G–4I) relative to the corresponding *Lar* transheterozygote (28%; $p < 0.01$). This indicates that removal of Sdc reduces the residual LAR function that is retained in zygotic *Lar*-null embryos.

We combined *Sara* and *Fkbp13* mutations with Lar^{bypass} in order to ensure that effects of *Sdc* mutations on these genes were not responsible for the increase in bypass frequency observed in *Lar Sdc* combinations. To determine if the interactions between *Lar* and *Sdc* were specific for this HSPG, or might be also observed for the other cell-surface HSPGs, we also examined double and triple mutants in which Lar^{bypass} was combined with *Dally* and *Dlp* mutations. In all of these cases, no increase in the frequency of the bypass phenotype over that seen in the *Lar* single mutant was observed (Figure S4A).

Sdc Expressed on Muscles Can Function as a Ligand for Neuronal LAR

LAR is an axonal protein enriched on growth cones [8, 31, 32] (Figure S5). ISNb axons begin to grow into the VLM field at mid-stage 15 [10]. We visualized Sdc expression at that time in order to determine whether it is appropriately localized to influence LAR-expressing growth cones entering the muscle field. Figures 5A and 5B show that Sdc is transiently expressed on patches of cells immediately adjacent to the growing ISNb nerve, consistent with the hypothesis that *trans* interactions between LAR and Sdc could regulate muscle field entry.

The genetic interaction results in Figure 4 suggest that Sdc is a positive regulator of LAR function, since the penetrance of the bypass phenotype in *Lar* LOF mutants increases when Sdc is removed. To obtain further information about how Sdc regulates LAR, we wished to devise a genetic test of whether Sdc can increase LAR signaling when expressed in *trans* to LAR. To do this, we first needed to define a gain-of-function (GOF) *Lar* axon guidance phenotype and then determine if this same phenotype can be produced by overexpressing Sdc on muscles. We could then perform an epistasis test, determining whether genetic removal of LAR function would be able to suppress the Sdc overexpression phenotype. If so, this would suggest that the axon guidance phenotype caused by Sdc overexpression arises through an increase in LAR's signaling activity mediated by interactions between muscle Sdc and neuronal LAR.

We first examined motor axons in embryos in which wild-type LAR was overexpressed in neurons, and we found guidance phenotypes affecting the SNa nerve. No ISNb phenotypes were observed. SNa axons leave the CNS in the SN root, and the nerve bifurcates dorsal to muscle 12 and splits into two branches that innervate muscles 21–24 (anterior branch) and muscles 5 and 8 (posterior branch) (Figures 6A and 6B). LAR overexpression from the elav-GAL4 driver produced SNa bifurcation phenotypes with a frequency of 23%. The anterior and posterior branches were equally likely to be affected (Figures 6C and 6F). This is a specific *Lar* GOF phenotype; *Lar* LOF mutants do not display SNa phenotypes ([11] and Figure S4A). However, *Ptp52F* LOF mutants display this same SNa phenotype, with a similar penetrance (28% for nulls). Interestingly, LAR and PTP52F have opposing activities in regulation of CNS axon guidance [12].

Generation of the *Lar* SNa GOF phenotype requires enzymatic activity, because overexpression of a LAR

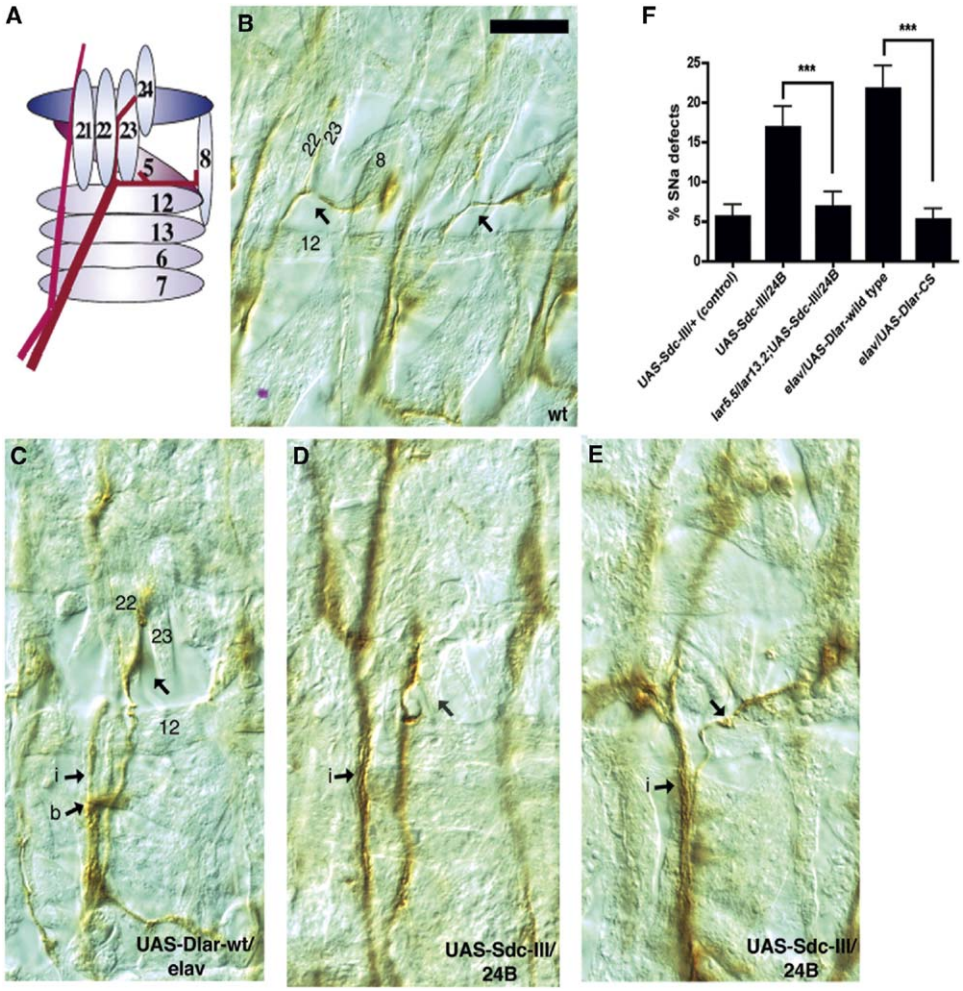

Figure 6. *trans* Interactions between Sdc and LAR Generate SNa Bifurcation Defects

(A) Schematic diagram of the SNa nerve and the surrounding muscles. SNa is shown in dark red, and the ISN is in pink. The SNa usually bifurcates at the ventral end of the cleft between muscles 22 and 23; it innervates muscles 5, 8, and 21–24. i, ISN; b, ISNb. Scale bar equals 5 μm.

(B–E) Each image shows one or two abdominal hemisegments of a late stage 16 embryo stained with mAb 1D4 using HRP immunohistochemistry and visualized with DIC optics (63× objective). Muscles are numbered in some panels.

(B) Hemisegments A4 and A5 of a wild-type embryo. Arrows indicate the SNa bifurcation points.

(C) Hemisegment A4 in an elav-GAL4 × UAS-LAR (LAR neuronal overexpression) embryo. The posterior branch of the SNa is missing. In (C)–(E), the arrows indicate the approximate points at which the SNa would have bifurcated if both branches were present.

(D) Hemisegment A3 in a 24B-GAL4 × UAS-Sdc (Sdc muscle overexpression) embryo. The posterior branch is missing.

(E) Hemisegment A3 in an Sdc muscle OE embryo. The anterior branch is missing.

(F) A bar graph showing the % of A2–A7 hemisegments that exhibit loss of at least one SNa branch in various genotypes. The numbers of hemisegments scored are as follows: UAS-Sdc-III/+ (isogenic control) = 206; UAS-Sdc-III/24B-GAL4 = 241; $Lar^{5.5}/Lar^{13.2}$;UAS-Sdc-III/24B-GAL4 = 124; elav-GAL4/UAS-Lar-wild-type = 159; elav-GAL4/UAS-Lar-C→S = 215. ***$p < 0.001$.

mutant with point mutations of the essential catalytic cysteine residues in both PTP domains does not produce SNa phenotypes at a greater frequency than the isogenic control (Figure 6F).

We then examined motor axon guidance in embryos overexpressing Sdc in muscles using the 24B-GAL4 driver and found identical SNa bifurcation phenotypes (Figures 6D–6F), with a penetrance of 18%; again, no ISNb phenotypes were observed. These results show that exposure of SNa motor axons to excess muscle Sdc causes bifurcation failures. We could now perform the key epistasis experiment, determining whether these phenotypes are suppressed when LAR is genetically removed from the motor axons. We introduced a *Lar* null mutant combination into lines in which Sdc is overexpressed in muscles. This completely suppressed the SNa bifurcation phenotype (to 7%, versus 6% for the isogenic UAS-Sdc insertion line control; Figure 6F; $p < 0.001$). These results indicate that Sdc on muscles can function in vivo as a ligand for LAR on motor axons and suggests that interaction in *trans* with Sdc increases LAR's signaling activity. Finally, to examine the specificity of the *Sdc* GOF phenotype, we also tested muscle overexpression of the glypicans Dally and Dlp using the

24B and G14 drivers. Dally overexpression produced SNa bifurcation phenotypes at a low penetrance (12%), while Dlp overexpression did not produce any phenotype (Figure S4B).

Discussion

In this paper, we identify the HSPG Sdc as a ligand for the RPTP LAR, a neuronal transmembrane receptor that regulates axon guidance in embryos and larvae. LAR interacts with the GAG chains of Sdc and binds to heparin and Sdc with nanomolar affinity (Figure 3). Genetic interaction studies using *Sdc* and *Lar* LOF mutations demonstrate that Sdc contributes to LAR's function in motor axon guidance (Figure 4). We also show that overexpression of Sdc on muscles generates the same phenotype as overexpression of LAR in neurons and that genetic removal of LAR suppresses the phenotype produced by ectopic Sdc (Figure 6). These results demonstrate that Sdc can interact with LAR in *trans* and suggest that Sdc is a positive regulator of LAR signaling in growth cones.

Using Deficiency Screens to Identify Ligands for Cell-Surface Receptors

We describe a new strategy for identification of ligand genes. First, the extracellular domain of the cell-surface receptor of interest is expressed as an AP fusion protein [33]. Second, the AP fusion protein is used to stain live-dissected *Drosophila* embryos to reveal the expression pattern of the putative ligand. Third, embryos homozygous for each of the deletion mutations in the Bloomington deficiency kit (which currently covers >92% of the genome) are dissected and stained with the AP fusion protein. If a deletion is identified that eliminates all or part of the staining pattern, overlapping deficiencies and insertion mutations can then be screened to isolate the gene responsible for the staining.

This type of screen has several advantages over expression cloning from cDNA library pools in transfected mammalian cells. First, expression cloning requires full-length cDNA clones and is thus difficult if the ligand mRNA is rare and/or large. This is not a concern with the deficiency screen, since one is searching for regions whose deletion eliminates staining, not for clones that confer staining. Second, if two or more subunits must come together to create a binding-competent ligand, this ligand will not be expressed by cells transfected with library pools, since any given pool would be unlikely to contain cDNAs for both subunits. However, the absence of a gene encoding one of the subunits would still be detected by the deficiency screen. Third, expression cloning is normally limited to cell-surface ligands, because soluble ligands would diffuse away from the transfected cell. The deficiency screen can permit cloning of genes encoding soluble ligands, as long as these remain attached to structures in the embryo during incubation with the AP fusion protein.

There are, however, several problems with the deficiency screen approach. First, about 1/4 of kit deficiencies cannot be screened because homozygous embryos have such severe phenotypes that staining patterns cannot be recognized. This is due to removal of genes (e.g., *Egfr* at 57E9; Table S1) whose zygotic expression is necessary for early development. To address this problem, we are examining smaller deletions in these "unscreenable regions" in order to narrow down the regions that cannot be screened to the smallest possible intervals around critical genes such as *Egfr*. Second, the deficiency screen does not necessarily locate the actual ligand genes; it would also identify regions encoding genes required for ligand synthesis. For example, deletion of the *ttv*, *sgl*, or *sfl* genes, which encode enzymes required for GAG synthesis, eliminates or reduces peripheral staining with LAR-AP, since these enzymes are necessary to make binding-competent Sdc. Finally, some receptors may recognize multiple ligands that are expressed in the same or similar patterns. In this case, a deletion removing the gene encoding one of these ligands might not perturb staining sufficiently to allow it to be identified in a screen. This is presumably the case for the second CNS ligand of LAR-AP (Figures 1 and 2). Sdc is also expressed on CNS axons; thus, a deficiency removing the CNS ligand would probably not eliminate axonal LAR-AP staining since Sdc would still be present in these embryos. To deal with this problem, we are now rescreening the deficiency kit with LAR-HS2-AP (Figures 2 and 3), a point mutant that cannot interact with Sdc.

Regulation of Motor Axon Guidance by Sdc

Genetic removal of Sdc from embryos bearing *Lar* mutations increases the penetrance of the characteristic *Lar* ISNb bypass phenotype. This effect on penetrance is as large as those usually observed when a second RPTP is genetically removed from a single *Rptp* mutant (e.g., removal of *DPTP69D* from a *Lar* mutant [10]).

Removal of Sdc increases penetrance for both hypomorphic and (zygotic) null *Lar* mutations (Figure 4). The effect on the null penetrance is likely due to reduction of maternally contributed LAR function [10]. However, we found that *Sdc* mutations alone do not produce ISNb bypass at a significant frequency, even when both maternal and zygotic Sdc are removed (Figure 4, Figure S4A). One explanation for this finding might be that Sdc is partially redundant with Dally and/or Dlp, since these are cell-surface HSPGs expressed in a similar pattern to Sdc.

To test this model, we reduced Dally and Dlp expression in an *Sdc* mutant background. It is difficult to assess the appropriate extent of reduction for this experiment. Glypicans cannot be completely removed, since this would produce embryos with severe early phenotypes due to loss of Hedgehog and Wingless signaling (reviewed by [15, 16]). We generated zygotic triple mutants (*Sdc dally dlp*), and we also injected *dally* and *dlp* dsRNAs into *Sdc* maternal/zygotic mutant embryos (*dally*/*dlp* RNAi would affect both maternal and zygotically contributed mRNAs). The genetic triple mutants had CNS phenotypes that are stronger than the *Sdc* phenotype [20, 21] but displayed few motor axon guidance errors. *Dally*/*Dlp*-injected *Sdc* mutant embryos had more severe phenotypes, but ISNb guidance was not selectively affected (data not shown). Overall, our data suggest that Sdc is not redundant with Dally or Dlp and that its absence is likely to be compensated

for by non-HSPG proteins. Perhaps the second LAR ligand that we detect by embryo staining is redundant with Sdc. Like Sdc, this ligand is expressed both on CNS axons and in lines in the periphery (Figure 2).

The genetic epistasis experiment of Figure 6 demonstrates that Sdc acts in *trans* (as a ligand) to regulate LAR function. However, these data allow us to reach this conclusion only for SNa bifurcation, which is affected by LAR overexpression but not by loss of LAR. In its regulation of the decision of ISNb growth cones to enter the muscle field, Sdc could also act as a ligand, since it is expressed at the appropriate time on patches of cells near the muscle field entry site that could be contacted by LAR-expressing ISNb growth cones at this choice point (Figure 5). Alternatively, Sdc could act as a coreceptor at this choice point since it is expressed on the motor nerves together with LAR. Finally, we do not know if the Sdc that interacts with LAR during ISNb axon guidance is attached to the cell surface or has been shed by proteolytic cleavage. If released Sdc is the essential ligand, this could be expressed by either muscles or neurons and transported to the choice point.

Conclusions

Our results show that the cell-surface HSPG Sdc is an in vivo ligand for LAR and indicate that it positively regulates LAR signaling during motor axon guidance. Sdc's GAG chains bind directly to LAR with high affinity, and this binding requires basic sequences in the first Ig domain of LAR. Further work will be required to determine whether binding to Sdc directly stimulates LAR's phosphatase activity, relocalizes LAR within the growth cone, or facilitates LAR signaling by another mechanism.

Experimental Procedures

Genetics

Sdc$^{Df(2R)48}$, generated by imprecise excision of *sdc^{10608}*, was previously described [20]. *Sdc^{KG06163}*, *Sdc^{10608}*, *sfl, sgl, ttv, pipe, trol, dally^{11685}*, *elav-Gal4*, *C155-Gal4*, *G14-Gal4*, *24B-Gal4*, and the deficiency kit strains were obtained from the Bloomington stock center. The *Fkbp13* allele *l(2)00734*, *Sara^{250}*, and ubi-Sara were obtained from M. O'Connor. *Lar^{bypass}* was obtained from D. Van Vactor. *dally^{80} dlp^{A187}* and UAS-Dlp were obtained from X. Lin. UAS-Lar-wt and UAS-Lar-C1638S-C1929S were obtained from N. Krueger. UAS-Dally lines were obtained from N. Perrimon's and S. Selleck's groups. UAS-Sdc insertions on chromosomes II and III were obtained from Tim Heslip. *Lar$^{13.2}$Sdc^{10608}* and *Lar$^{5.5}$Sdc^{Df48}* were obtained from Karl Johnson. Deficiency kit lines were balanced over *FM7c, P{GAL4-Kr.C}DC1,P{UAS-GFP.S65T}DC5,sn^{-}*, *CyOarmGFP*, or *TM3armGFP*.

Immunohistochemistry

The desired mutant embryos were identified based on the absence of staining with rabbit-anti-GFP (Molecular Probes; 1:1000), which detects the presence of the GFP gene on the balancer chromosomes. mAb 1D4 [34] was used at 1:3 dilution to reveal motor axon and CNS pathways, dissected, and photographed with a Magnafire digital camera on a Zeiss Axioplan microscope using Nomarski optics. Antibody staining using HRP immunohistochemistry was performed as described [35].

Rabbit anti-Sdc was a gift from Tim Heslip and John Lincecum. Anti-Dlp mAb supernatant was obtained from the Developmental Studies Hybridoma Bank. Anti-Myc (Sigma; clone 9E10 [ascites fluid]) was used at 1:250. Secondary antibodies conjugated to either Alexa 488 or Alexa 568 (Molecular Probes) were used to visualize antibody staining in the embryos.

Binding Experiments

RPTP-AP fusion proteins were incubated with 10 μl (3.7 μg heparin) heparin-agarose beads (Sigma; preblocked with 1×PBS + 3% bovine serum albumin [BSA] for 1 hr at room temperature) or with Kc167 cells (*Drosophila* Genomics Resources Center, Indiana University) or S2 cells (10 × 10^6 cells) for 3 hr at room temperature. Heparin-agarose beads or cells were washed extensively with HBAH (Hanks' balanced salt solution: BSA [0.5 mg/ml], 0.1% [w/v] NaN_3, 20 mM HEPES [pH 7.0]). Heparin-agarose beads were resuspended in 1× Hanks buffered saline (HBS: 150 mM NaCl, 20 mM HEPES [pH 7.0]), and cells were lysed with Triton-Tris lysis buffer (1% Triton X-100, 10 mM Tris [pH 8.0]). Endogenous alkaline phosphatase (AP) activity of the samples was quenched by a 10 min incubation at 65°C. AP activity was determined by adding SEAP buffer (0.5 mM $MgCl_2$, 1 M diethanolamine [pH 9.8]) containing 1 mg/ml *p*-nitrophenyl phosphate (Sigma). Progress curves were recorded every 5 min for 1 hr at room temperature at 405 nm on an EL312e biokinetics reader (Bio-Tek Instruments), and maximum rates were determined by Delta Soft 3 software (version 2.243, Bio-Tek Instruments). Each data point represents the average of triplicate reactions. Curves were generated using GraphPad Prism 4 software (GraphPad Software). Figure 3 data were normalized against the amount of input AP fusion proteins, determined by immunoprecipitation of the AP fusion proteins with anti-PLAP and protein A/G beads followed by an AP assay, described above.

Transient Transfections

HEK 293T cells were transiently transfected with pCMV-FLAG-Sdc-ECD (extracellular domain: aa 29–335) by use of FuGENE6 transfection reagent (Roche). This construct has the endogenous Sdc signal sequence deleted and replaced with the gp67 signal sequence, and a C-terminal FLAG tag has been fused to the end of the Sdc ECD at aa 335. 48 hr after transfection, conditioned media were collected and subjected to coimmunoprecipitation and other binding assays.

Coimmunoprecipitation Assays

Conditioned media from HEK 293T cells transiently transfected with pCMV-FLAG-Sdc-ECD were incubated with Lar-AP fusion protein, anti-FLAG M2 mAb (Sigma), or anti-PLAP polyclonal antibody and Protein G Plus/Protein A-agarose beads (Oncogene Research Products). After 1 hr incubation at 4°C of conditioned media and LAR-AP, anti-FLAG mAb and Protein G Plus/Protein A-agarose beads were added. After one more incubation at 4°C, the Protein G Plus/Protein A-agarose beads were extensively washed and subjected to SDS-PAGE and Western blotting. The Western blot was probed with anti-PLAP polyclonal antibody, goat-anti-rabbit-alkaline phosphatase secondary (Jackson Immunoresearch) and detected with NBT/BCIP.

Supplemental Data

Supplemental Data include five figures, one table, and Supplemental Experimental Procedures and can be found with this article online at http://www.current-biology.com/cgi/content/full/15/19/1701/DC1/.

Acknowledgements

We thank Aloisia Schmid for many contributions to the ligand project; Anya Vlasak and Violana Nesterova for technical assistance; Peter Snow and Inderjit Nangiana of the Caltech Protein Expression Facility for fusion proteins; John Thomas for discussions on fusion protein staining of embryos; David Chang for assistance with mammalian transfection; Devin Tesar, Andrew Tapper, and Pamela Bjorkman for discussions on in vitro binding experiments; members of the Zinn group for other helpful discussions; Tim Heslip and Michael O'Connor for communication of unpublished results on Sdc; David Van Vactor, John Flanagan, Karl Johnson, and Alan Tenney for communicating their results prior to publication; and Karl

Johnson for unpublished *Drosophila* lines. We thank Tim Heslip, Michael O'Connor, David Van Vactor, John Flanagan, Xinhua Lin, Scott Selleck, Norbert Perrimon, Hiroshi Nakato, John Lincecum, Gerd Vorbruggen, and Daniela Dieterich for essential fly stocks, antibody reagents, and AP fusion proteins. We thank the Developmental Studies Hybridoma Bank (DSHB) for its repository of available antibodies. K.Z. thanks Brad Olwin, Tin Tin Su, and Leslie Leinwand for hospitality and lab space during a sabbatical at the University of Colorado, where some of this work was performed. This work was supported by an RO1 grant to K.Z., NS28182. A.N.F. was supported by an NIH postdoctoral fellowship. We dedicate this paper to the memory of Peter M. Snow.

Received: August 3, 2005
Accepted: August 4, 2005
Published: October 11, 2005

References

1. Beltran, P.J., and Bixby, J.L. (2003). Receptor protein tyrosine phosphatases as mediators of cellular adhesion. Front. Biosci. *8*, D87–D99.
2. Meng, K., Rodriguez-Pena, A., Dimitrov, T., Chen, W., Yamin, M., Noda, M., and Deuel, T.F. (2000). Pleiotrophin signals increased tyrosine phosphorylation of beta-catenin through inactivation of the intrinsic catalytic activity of the receptor-type protein tyrosine phosphatase beta/zeta. Proc. Natl. Acad. Sci. USA *97*, 2603–2608.
3. Peles, E., Schlessinger, J., and Grumet, M. (1998). Multi-ligand interactions with receptor-like protein tyrosine phosphatase beta: implications for intercellular signaling. Trends Biochem. Sci. *23*, 121–124.
4. O'Grady, P., Thai, T.C., and Saito, H. (1998). The laminin-nidogen complex is a ligand for a specific splice isoform of the transmembrane protein tyrosine phosphatase LAR. J. Cell Biol. *141*, 1675–1684.
5. Sajnani-Perez, G., Chilton, J.K., Aricescu, A.R., Haj, F., and Stoker, A.W. (2003). Isoform-specific binding of the tyrosine phosphatase PTPsigma to a ligand in developing muscle. Mol. Cell. Neurosci. *22*, 37–48.
6. Aricescu, A.R., McKinnell, I.W., Halfter, W., and Stoker, A.W. (2002). Heparan sulfate proteoglycans are ligands for receptor protein tyrosine phosphatase sigma. Mol. Cell. Biol. *22*, 1881–1892.
7. Johnson, K.G., and Van Vactor, D. (2003). Receptor protein tyrosine phosphatases in nervous system development. Physiol. Rev. *83*, 1–24.
8. Krueger, N.X., Van Vactor, D., Wan, H.I., Gelbart, W.M., Goodman, C.S., and Saito, H. (1996). The transmembrane tyrosine phosphatase DLAR controls motor axon guidance in *Drosophila*. Cell *84*, 611–622.
9. Desai, C.J., Gindhart, J.G., Jr., Goldstein, L.S.B., and Zinn, K. (1996). Receptor tyrosine phosphatases are required for motor axon guidance in the *Drosophila* embryo. Cell *84*, 599–609.
10. Desai, C.J., Krueger, N.X., Saito, H., and Zinn, K. (1997). Competition and cooperation among receptor tyrosine phosphatases control motoneuron growth cone guidance in *Drosophila*. Development *124*, 1941–1952.
11. Sun, Q., Schindelholz, B., Knirr, M., Schmid, A., and Zinn, K. (2001). Complex genetic interactions among four receptor tyrosine phosphatases regulate axon guidance in *Drosophila*. Mol. Cell. Neurosci. *17*, 274–291.
12. Schindelholz, B., Knirr, M., Warrior, R., and Zinn, K. (2001). Regulation of CNS and motor axon guidance in *Drosophila* by the receptor tyrosine phosphatase DPTP52F. Development *128*, 4371–4382.
13. Desai, C., and Purdy, J. (2003). The neural receptor protein tyrosine phosphatase DPTP69D is required during periods of axon outgrowth in *Drosophila*. Genetics *164*, 575–588.
14. Spring, J., Paine-Saunders, S.E., Hynes, R.O., and Bernfield, M. (1994). *Drosophila* syndecan: conservation of a cell-surface heparan sulfate proteoglycan. Proc. Natl. Acad. Sci. USA *91*, 3334–3338.
15. Kramer, K.L., and Yost, H.J. (2003). Heparan sulfate core proteins in cell-cell signaling. Annu. Rev. Genet. *37*, 461–484.
16. Selleck, S.B., and Nakato, H. (2004). Functional dissection of glyco-conjugates during development: lessons from the fruitfly. Trends Glycosci. Glycotechnol. *16*, 95–108.
17. Lee, J.S., and Chien, C.B. (2004). When sugars guide axons: insights from heparan sulphate proteoglycan mutants. Nat. Rev. Genet. *5*, 923–935.
18. Holt, C.E., and Dickson, B.J. (2005). Sugar codes for axons? Neuron *46*, 169–172.
19. Lee, J.S., von der Hardt, S., Rusch, M.A., Stringer, S.E., Stickney, H.L., Talbot, W.S., Geisler, R., Nusslein-Volhard, C., Selleck, S.B., Chien, C.B., et al. (2004). Axon sorting in the optic tract requires HSPG synthesis by *ext2* (*dackel*) and *extl3* (*boxer*). Neuron *16*, 947–960.
20. Johnson, K.G., Ghose, A., Epstein, E., Lincecum, J., O'Connor, M.B., and Van Vactor, D. (2004). Axonal heparan sulfate proteoglycans regulate the distribution and efficiency of the repellent slit during midline axon guidance. Curr. Biol. *14*, 499–504.
21. Steigemann, P., Molitor, A., Fellert, S., Jackle, H., and Vorbruggen, G. (2004). Heparan sulfate proteoglycan syndecan promotes axonal and myotube guidance by slit/robo signaling. Curr. Biol. *14*, 225–230.
22. Flanagan, J.G., Cheng, H.J., Feldheim, D.A., Hattori, M., Lu, Q., and Vanderhaeghen, P. (2000). Alkaline phosphatase fusions of ligands or receptors as in situ probes for staining of cells, tissues, and embryos. Methods Enzymol. *327*, 19–35.
23. Toyoda, H., Kinoshita-Toyoda, A., Fox, B., and Selleck, S.B. (2000). Structural analysis of glycosaminoglycans in animals bearing mutations in *sugarless, sulfateless*, and *tout-velu*. J. Biol. Chem. *275*, 21856–21861.
24. Nakato, H., Futch, T.A., and Selleck, S.B. (1995). The *division abnormally delayed* (*dally*) gene: a putative integral membrane proteoglycan required for cell division patterning during postembryonic development of the nervous system in *Drosophila*. Development *121*, 3687–3702.
25. Khare, N., and Baumgartner, S. (2000). Dally-like protein, a new *Drosophila* glypican with expression overlapping with *wingless*. Mech. Dev. *99*, 199–202.
26. Park, Y., Rangel, C., Reynolds, M.M., Caldwell, M.C., Johns, M., Nayak, M., Welsh, C.J.R., McDermott, S., and Datta, S. (2003). *Drosophila* Perlecan modulates FGF and Hedgehog signals to activate neural stem cell division. Dev. Biol. *253*, 247–257.
27. Voigt, A., Pflanz, R., Schafer, U., and Jackle, H. (2002). Perlecan participates in proliferation activation of quiescent *Drosophila* neuroblasts. Dev. Dyn. *224*, 403–412.
28. Hileman, R.E., Fromm, J.R., Weiler, J.M., and Linhardt, R.J. (1998). Glycosaminoglycan-protein interactions: definition of consensus sites in glycosaminoglycan binding proteins. Bioessays *20*, 156–167.
29. Vaughn, D.E., and Bjorkman, P.J. (1997). High-affinity binding of the neonatal Fc receptor to its IgG ligand requires receptor immobilization. Biochemistry *36*, 9374–9380.
30. Krueger, N.X., Reddy, R.S., Johnson, K., Bateman, J., Kaufmann, N., Scalice, D., Van Vactor, D., and Saito, H. (2003). Functions of the ectodomain and cytoplasmic tyrosine phosphatase domains of receptor protein tyrosine phosphatase Dlar in vivo. Mol. Cell. Biol. *23*, 6909–6921.
31. Tian, S.-S., Tsoulfas, P., and Zinn, K. (1991). Three receptor-linked protein-tyrosine phosphatases are selectively expressed on central nervous system axons in the *Drosophila* embryo. Cell *67*, 675–685.
32. Sun, Q., Bahri, S., Schmid, A., Chia, W., and Zinn, K. (2000). Receptor tyrosine phosphatases regulate axon guidance across the midline of the *Drosophila* embryo. Development *127*, 801–812.
33. Flanagan, J.G., and Cheng, H.J. (2000). Alkaline phosphatase fusion proteins for molecular characterization and cloning of receptors and their ligands. Methods Enzymol. *327*, 198–210.
34. Van Vactor, D., Sink, H., Fambrough, D., Tsoo, R., and Goodman, C.S. (1993). Genes that control neuromuscular specificity in *Drosophila*. Cell *73*, 1137–1153.
35. Patel, N.H. (1994). Imaging neuronal subsets and other cell types in whole-mount Drosophila embryos and larvae using antibody probes. In *Drosophila melanogaster*: Practical Uses in Cell and Molecular Biology, Volume 44, E. Fyrberg and L.S.B. Goldstein, eds. (San Diego, CA: Academic Press), pp. 446–488.